Journal of Geochemical Exploration 242 (2022) 107091

Contents lists available at ScienceDirect

Journal of Geochemical Exploration

journal homepage: www.elsevier.com/locate/gexplo

Solving geological mixing problems with Bayesian tracer models: A demonstration of the method applied to Carlin-type pyrite

E.A. Holley [a,*], D.L. Phillips [b]

[a] Department of Mining Engineering, Colorado School of Mines, 1600 Illinois Street, Golden, CO 80401, United States
[b] EcoIsoMix, Corvallis, OR 97330, United States

ARTICLE INFO

Keywords:
Bayesian tracer model
Mixing
Stable isotopes
Carlin-type gold

ABSTRACT

Mixing problems are common in ore deposit geochemistry, since numerous geological sources can contribute metals and other elements during mineralization. Here we demonstrate how Bayesian tracer models from the field of ecology can be used to solve geochemical mixing problems in the study of ore deposits. The model MixSIAR (Mixing Stable Isotope Analysis in R) was developed by ecologists to quantify the proportional contributions to a consumer's diet, using stable isotopic tracers for the consumer and its potential diet sources. In a novel application of MixSIAR, we adapt the method to solve mixing problems in ore deposit genesis. We treat hydrothermal ore minerals as the mixtures and the potential fluids as the sources, enabling us to model the probability distributions of source contributions to the ore minerals. We use Carlin-type pyrite as our example, since the Au enrichment in the pyrite has been alternately suggested to record the circulation of meteoric fluids through a metalliferous package of sedimentary rocks, or the exsolution and ascent of Au-rich fluids from Eocene magmas. Using $\delta^{34}S$ as a tracer and Au as a covariate, we model the contributions of four potential sources to Carlin-type hydrothermal pyrite: local sedimentary pyrite, unmineralized Popovich Formation stratigraphy, Jurassic and Cretaceous granitoids, and Eocene magmatic fluids. The modeling indicates that all these sources likely contributed during hydrothermal pyrite growth, and the proportional contribution of Eocene magmatic fluid is positively correlated with Au. We briefly compare the model to other methods, in order to illustrate how Bayesian tracer modeling is ideally suited to study mineralization and other geological processes.

1. Introduction

Mixing problems are common research challenges in the study of ore deposits. Hydrothermal systems typically involve mixing between two or more fluid sources, or interactions between one or more fluids and numerous rock types. The resulting alteration and ore minerals have mixed signatures, potentially obfuscating the individual source contributions and the causative mineralizing processes. Similarly, the stream sediment geochemistry datasets used in mineral exploration are mixing problems, recording water-rock interaction in tributaries followed by fluid mixing in larger downstream catchments, and it is important to determine the relative trace element contributions of each tributary. Here we present a novel application of ecological Bayesian tracer mixing models, demonstrating how they can be used to solve mixing problems in geological studies of mineral deposits. We use Carlin-type pyrite as an example to demonstrate the utility of the method, modeling the relationship between trace element concentration and source contribution during mineralization.

Bayesian tracer mixing models were originally developed for food web studies, enabling ecologists to identify the diet proportions of consumers (e.g., wolf packs), by comparing the $\delta^{15}N$ and $\delta^{13}C$ stable isotope compositions of the consumer or predator's tissue or stomach contents to the compositions of tissues from potential prey populations (e.g., deer, marine mammals, and salmon; Semmens et al., 2009; Parnell et al., 2013; Phillips et al., 2014; Stock et al., 2018). Like the consumer in a food-web study, mineral deposits are mixtures, with geochemical components derived from various sources. This modeling approach has not been previously used to examine mineralizing processes. We show that Bayesian tracer models are easily adapted to the disciplinary context.

To demonstrate the utility of Bayesian tracer modeling, we apply the method to a well-known mixing problem in economic geology: the origins of Carlin-type gold. The Au-bearing hydrothermal pyrites in Carlin-type deposits have been alternately suggested to record meteoric fluid

* Corresponding author.
E-mail address: eholley@mines.edu (E.A. Holley).

https://doi.org/10.1016/j.gexplo.2022.107091
Received 8 June 2022; Received in revised form 23 August 2022; Accepted 16 September 2022
Available online 21 September 2022

circulation through a metalliferous package of sedimentary rocks (Hofstra, 1994, 1995; 1999; Ilchik and Barton, 1997; Emsbo et al., 1999, 2003; Hofstra and Cline, 2000; Large et al., 2011), or the exsolution and ascent of fluids from Eocene magmas (Sillitoe and Bonham, 1990; Henry and Boden, 1998; Ressel et al., 2000; Johnston and Ressel, 2004; Seedorff and Barton, 2004; Muntean et al., 2011). The timing of deposit formation generally tracks the southwest sweep of Eocene magmatism through the Great Basin (Cline et al., 2005; Ressel and Henry, 2006), and it is clear that both magmatic and meteoric fluids were circulating at the time of mineralization. Various trace element, stable isotope, and fluid inclusion datasets support one model or the other, or both. Most recently, Holley et al. (2022) collected the first standardized NanoSIMS analyses of $\delta^{34}S$ and trace elements of Carlin-type pyrite to show that although both magmatic and meteoric fluids contributed to the ore, the $\delta^{34}S$ values of gold-rich nanoscale pyrite zones are similar to those of Eocene magmas.

Despite the prevalence of mixed signatures in geochemical data from Carlin-type deposits, no studies have focused on examining the mixing. Indeed, quantitative analysis of multi-component mixing has been rare in studies on ore deposit genesis or petrogenesis. Most commonly, studies assume two-component mixing and assess this qualitatively (e.g., Fusswinkel et al., 2013), graphically by interpolating mixing trends between end member compositions on X-Y plots (e.g., Gray, 1984; Hofstra and Cline, 2000; Rottier et al., 2021), or by simple ratio calculations (e.g., Schwinn et al., 2006). The most sophisticated quantitative approach is by Lesher and Burnham (2001), who used multicomponent mass-balance equations to model isotopes and elements in magmatic Ni-Cu-(PGE) systems. More advanced statistical methods are more common in stream sediment geochemistry, where catchment analysis (e.g., Hawkes, 1976; Bonham-Carter et al., 1987; Carranza and Hale, 1997; Carranza, 2009), multiple regression experiments (e.g., Bonham-Carter and Goodfellow, 1986), and machine learning (e.g., Grunsky and Arne, 2020) have become standard practice to calculate the source contributions to a geochemical mixture. However, to our knowledge, Bayesian statistics have not been used to solve geochemical mixing problems in ore deposit genesis, stream sediment studies, or any related application. Relative to graphical methods and simple two-component mixing calculations, Bayesian statistics have the advantage of providing actual probability distributions for source proportion estimates; furthermore, they can include larger numbers of sources, and incorporate information from uncertainties, prior estimates, and covariates (Stock et al., 2018). In the present contribution, we use Bayesian stable isotopic mixing models to calculate the probability distributions of source contributions during hydrothermal mineralization. Our modeling shows that the relative contributions of magmatic and meteoric fluids varied during Carlin-type ore pyrite growth, and that the modeled proportional contribution of Eocene magmatic fluid is positively correlated with Au enrichment of the pyrite.

2. Stable isotopic mixing models

Mixing models quantify the proportional contributions of multiple sources to a mixture of those sources based on the value of one or more chemical tracers. For example, stable isotope ratios in a mixture (e.g., $\delta^{13}C$ or $\delta^{15}N$ for ecological studies, or $\delta^{34}S$ for ores) reflect the stable isotope composition of the sources weighted by their mass contributions. Tracer mixing models are fundamentally based on the equations:

$$Y_j = \sum_k p_k \mu^s_{jk}$$

$$\Sigma p_k = 1$$

For each of j tracers, the mean tracer value of the mixture, Y_j, equals the sum of the k source tracer means, μ^s_{jk}, multiplied by their proportional contributions to the mixture, p_k. When the number of sources k is one more than the number of tracers j, this corresponds to a system of k equations with k unknowns (p_k), which has a unique analytical solution, and error propagation calculations have been used to establish confidence intervals around the estimated proportions (IsoError - Phillips and Gregg, 2001a, 2001b). If there are more than $j + 1$ sources (an underdetermined system of equations), then some of the sources may be aggregated to preserve the analytically solvable system (Phillips et al., 2005). Alternatively, all combinations of the $j + 1$ sources can be tested to determine which ones reproduce the observed mixture tracer means (IsoSource - Phillips and Gregg, 2003). This results not in single estimates of source proportions, but distributions of possible ones. More recently, Bayesian mixing models have been developed that estimate probability distributions for source contributions accounting for prior information, uncertainty in source and mixture isotopic signatures, and can be used in underdetermined mixing systems (Moore and Semmens, 2008; Parnell et al., 2010). These methods involve randomly generating q vectors of possible proportional source contributions ($\mathbf{f}_q$). Using Bayes theorem, the probability of each $\mathbf{f}_q$ given the data is calculated based both on the observed data and on prior information about the expected contributions (Ellison, 2004):

$$P(\mathrm{f_q}|\mathrm{data}) = \frac{L(\mathrm{data}|\mathrm{f_q}) * P(\mathrm{f_q})}{\sum L(\mathrm{data}|\mathrm{f_q}) * P(\mathrm{f_q})}$$

where $L(\mathrm{data}|\mathbf{f}_q)$ is the likelihood of the data given $\mathbf{f}_q$, and $P(\mathbf{f}_q)$ is the probability of $\mathbf{f}_q$ based on prior information about source proportions. Priors may be uninformative, where all source contributions are considered equally likely, or informative, where this is not the case. Prior probability distributions are specified using the Dirichlet distribution (Stock et al., 2018). Model fitting is by Markov Chain Monte Carlo (MCMC) and the resulting source contribution posterior distributions are true probability density distributions which account for both the data and prior information (Parnell et al., 2010).

Various adaptations of Bayesian stable isotopic models have been developed to account for hierarchical structure in food webs (Semmens et al., 2009), uncertainty in the mean and variance of the sources (Ward et al., 2010), and other covariate factors (Francis et al., 2011). Similar models have been used to fingerprint sediment erosion and pollution (e.g., Blake et al., 2018; Torres-Martínez et al., 2020). We use the model MixSIAR (Mixing Stable Isotope Analysis in R; Stock et al., 2018) which unifies these parameterizations in the R environment for statistical computing. The model is a combination of MixSIR, where SIR refers to Sampling-Importance-Resampling (Moore and Semmens, 2008), and SIAR which stands for Stable Isotope Analysis in R (Parnell et al., 2010). Using MCMC simulation on stable isotope and trace element geochemical data from minerals in the ore deposits and the potential source reservoirs, we calculate the probability distributions of fluid and metal source contributions during hydrothermal mineralization in Nevada's Carlin-type deposits. When combined with input data of sufficiently high spatial resolution, Bayesian mixing models are a powerful tool to decipher the contributions of individual geologic processes operating in complex systems.

3. Geologic setting

Carlin-type deposits occur on five main trends in northern Nevada (Fig. 1) and are the source of nearly 80 % of the gold produced in the United States (Perry and Visher, 2016). They are also potential resources of arsenic and antimony (Goldfarb et al., 2016), both defined as critical minerals of strategic importance (USGS, 2022). Carlin-type deposits are hydrothermal replacement bodies of stratigraphically and structurally controlled disseminated ore, hosted primarily in decarbonized silty carbonates and limey mudstones below less permeable siliciclastic rocks (Cline et al., 2005). Several deposits occur at the margins of Jurassic or Cretaceous intrusions, such as the Goldstrike stock on the northern Carlin trend, or the Osgood stock on the Getchell trend. Eocene dikes are volumetrically minor at some deposits and are unrecognized at others.

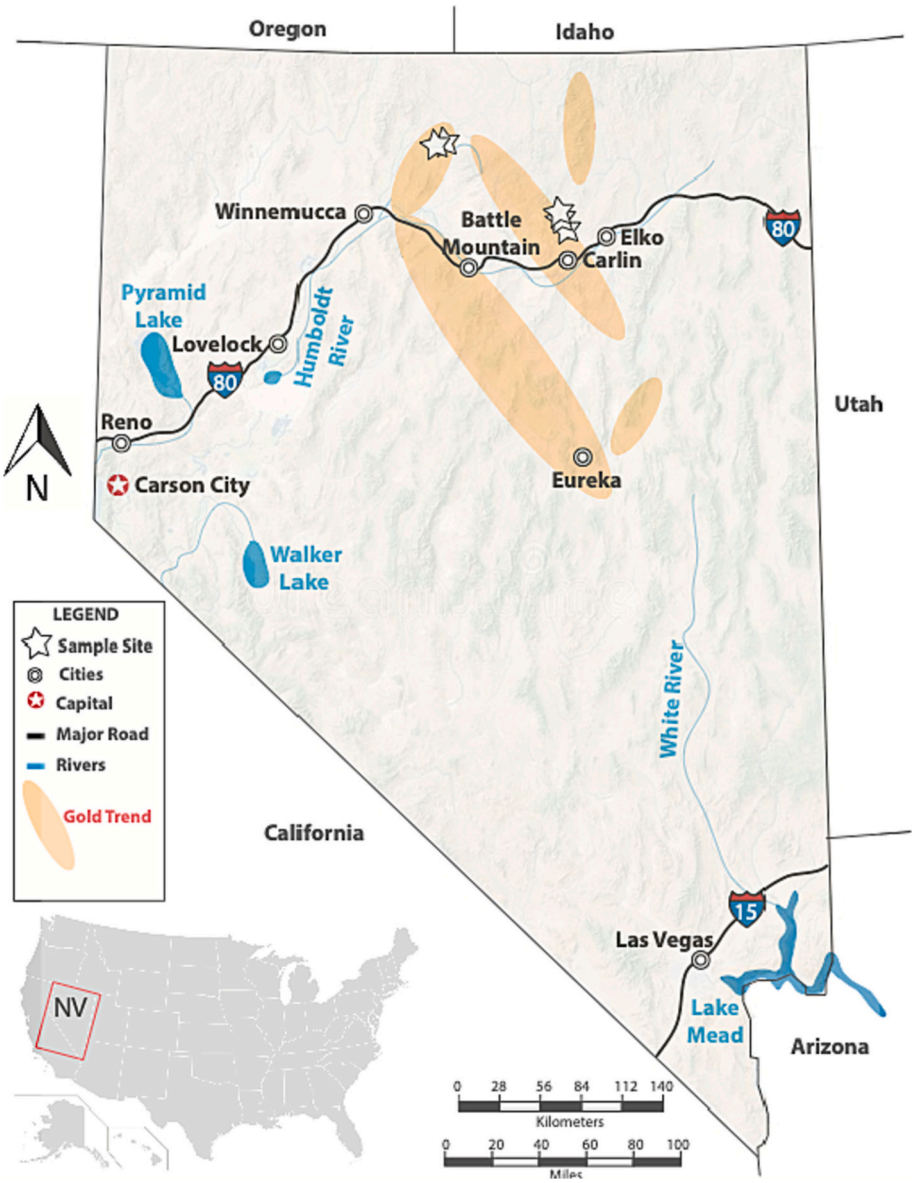

Fig. 1. Location of the five main trends hosting Carlin-type gold deposits in Nevada, modified from Huff et al. (2020). (For interpretation of the references to colour in this figure legend, the reader is referred to the web version of this article.)

In deposits that remain unoxidized by near-surface processes, precursor pyrite grains are rimmed by micron to submicron-scale hydrothermal arsenian pyrite that hosts "invisible gold" in solid solution or as nanoparticles. The lack of abundant hydrothermal alteration minerals and the small size of the hydrothermal pyrites have made it difficult to study the processes responsible for Carlin-type mineralization (Richards, 2011).

4. Input data for the model

Since reduced sulfur was the main ligand for Au during Carlin-type mineralization, the sulfur isotopic signature of the hydrothermal pyrite can be used to examine the potential sources of the Au. For the Bayesian tracer modeling, we compiled previously published $\delta^{34}S$ data from potential source reservoirs, as well as Carlin-type pyrite from five Carlin-type gold deposits in northern Nevada: the Getchell and Turquoise Ridge deposits on the Getchell trend, and the Beast, Deep Star, and Carlin deposits on the northern Carlin trend. In the following subsections, we describe how we defined the "mixtures," "sources," and "tracers" that we used as model inputs. Then we explain how to execute the modeling in the section on Modeling Methods.

4.1. Mixtures

We defined Carlin-type hydrothermal ore pyrites as the "mixtures" in our modeling. These hydrothermal pyrites represent mixtures of geochemical components derived from various potential sources, analogous to the predator that consumes various prey in a food web study. The modeling allows us to establish the probability distributions of potential source contributions to the ore pyrites during hydrothermal mineralization. In another example of a geological application, in a stream sediment study the mixtures are the samples from high-order drainages in a watershed; these mixtures receive inputs from multiple tributary sources.

The MixSIAR model accommodates an unlimited number of analytes, or "tracers" associated with each mixture or source data point. In food web studies, the most common tracers are $\delta^{13}C$ and $\delta^{15}N$. Elemental concentrations can also be used as tracers, and such an approach could be taken in a stream sediment study. In our modeling of Carlin-type pyrite, we used $\delta^{34}S$ as our tracer, expressed in delta notation (δ)

(Krouse and Coplen, 1997) relative to Vienna Cañon Diablo Troilite VCDT, in per mil (‰). We used the $\delta^{34}S$ values from previously published NanoSIMS analyses of Carlin-type hydrothermal pyrites (Holley et al., 2022), since these are the highest spatial resolution standardized data available. The $\delta^{34}S$ values vary by deposit, and there is also variation in nanoscale zones within individual grains (Fig. 2). The entire $\delta^{34}S$ dataset for the hydrothermal pyrites ranged from 45.2 ‰ to −1.3 ‰ (Appendix 1). For the modeling we divided the data into five groups by location: Getchell, Carlin, Turquoise Ridge, Deep Star, and Beast. The MixSIAR model allows input of raw data or means and standard deviations for each mixture and source population, and throughout our study we elected to use the raw data to capture subtle relationships in the dataset. The model cannot accommodate uncertainties associated with individual datapoints.

The stable isotope signatures of many ore and alteration minerals display temperature-dependent fractionation relative to the mineralizing fluid, which must be taken into account when modeling potential fluid source contributions to those minerals. We used the published $\delta^{34}S$ values for Carlin-type hydrothermal pyrites to calculate the $\delta^{34}S$ of fluids in equilibrium with those pyrites. We used the pyrite-H_2S fractionation equation of Ohmoto and Rye (1979) at 200 °C, which is a reasonable estimate for the temperature of Carlin-type mineralization (Cline et al., 2005). This correction resulted in $\delta^{34}S_{fluid}$ values ranging from 43.4 ‰ to −3.1 ‰, and we used these data as our mixture tracer data points (Appendix 1). The MixSIAR model allows the user to specify fractionation between the source and the consumer, which can vary according to trophic level, but we found it more straightforward to correct our data for fractionation in a spreadsheet outside the modeling framework.

We were particularly interested in the relationship between Au concentrations and $\delta^{34}S$ in Carlin-type pyrite, but relatively few of the data sets from potential sources contain both $\delta^{34}S$ and high spatial resolution trace element values of pyrite (see Sources below). In situations where a mixture data set contains additional attributes beyond those available for the source data sets, the MixSIAR model allows the user to include these as covariates. This approach was designed for ecological applications such as study of zooplankton diet, where $\delta^{13}C$ and $\delta^{15}N$ tracer data are available for the sources and the zooplankton mixtures, and the relative source contributions vary with an external factor such as Secchi depth (cloudiness) of the water body in the location where the zooplankton occur (Francis et al., 2011; Stock, 2022). The covariate feature of MixSIAR is particularly useful for ore deposits, since relative source contributions during mineralization may vary according to factors such as depth, host rock composition, proximity to structures, or other features that are not necessarily relevant descriptors for the sources.

We defined the Au concentration of the hydrothermal pyrite as a continuous covariate for each mixture data point in MixSIAR, using Au data collected simultaneously with sulfur during NanoSIMS spot analyses (Fig. 2; Appendix 1). Since the trace metal concentrations of validated $\delta^{34}S$ standards are not known at the nanoscale, Holley et al. (2022) used the established method of Zhang et al. (2017) to calculate the Au concentrations of the pyrites according to relative sensitivity factors calibrated using the electron microprobe. The Au concentrations varied widely between individual geochemical zones of the hydrothermal pyrites, ranging from 0.1 ppm to 1709 ppm. Holley et al. (2022) observed a general correlation between $\delta^{34}S$ and Au concentration of the pyrite: within groups of samples from the same deposit, the highest Au concentrations were associated with $\delta^{34}S$ values in the range of $\delta^{34}S$ for Eocene magmas and Eocene magmatic-hydrothermal sulfides in the region. The same trend was observable within individual grains,

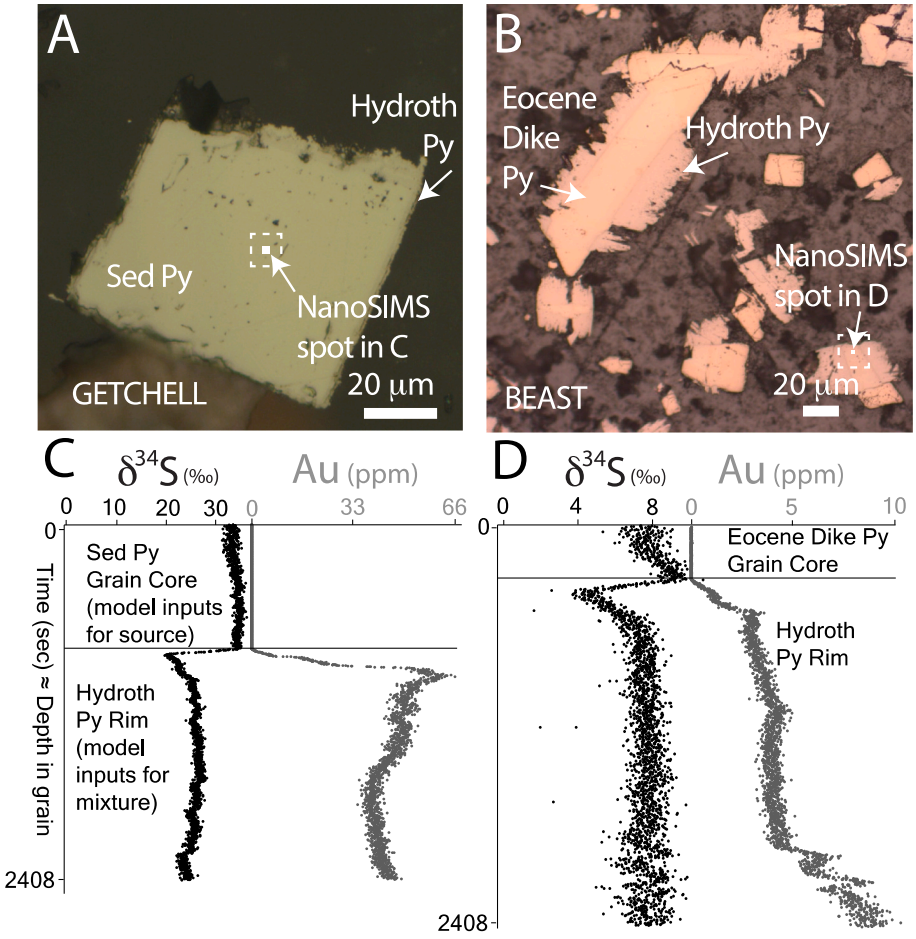

Fig. 2. Examples of input data for the MixSIAR model (data modified from Holley et al., 2022). Reflected light images show NanoSIMS spot locations on precursor pyrite grains rimmed by Carlin-type hydrothermal pyrite from (A) Getchell, and (B) Beast. The NanoSIMS $\delta^{34}S$ and Au depth profiles from (C) Getchell and (D) Beast can be read like drill hole logs: the analyses commence in the precursor pyrite at the grain surface and penetrate into the underlying hydrothermal pyrite rim which is internally zoned with respect to Au concentration. Zones of consistent composition were averaged to produce plateau data points used as mixture and source data points for the model, in addition to literature data for other potential sources of sulfur and metals.

wherein growth zones of higher Au concentrations had $\delta^{34}S$ values closest to the Eocene magmatic values. The MixSIAR modeling allows us to quantitatively test this trend.

4.2. Sources

The tracer compositions of a mixture must be compared to those of potential sources. In a food web study, the sources are the prey. In a stream sediment study, the sources would be the rocks in the upstream catchments. In geological studies of ore deposits, the sources are the various reservoirs from which metals and ligands could have been derived, which might include *syn*-mineralization magmatic intrusions; older metamorphic, magmatic or magmatic-hydrothermal units present in the host rocks; sedimentary rocks in distal, overlying, or underlying stratigraphy; or other fluids present in or generated by these rocks. We considered three general types of sources which may have contributed sulfur and metals to Carlin-type hydrothermal pyrite (Table 1; Appendix 1), and we discuss each in detail here.

4.2.1. Sedimentary rocks

The sedimentary host rock package in northern Nevada includes metalliferous horizons, sulfur-bearing minerals, and organosulfur complexes that could have been scavenged and then redeposited during fluid circulation. The potential sedimentary contributions to Carlin-type mineralization are the most challenging model inputs to define for two reasons: a comprehensive $\delta^{34}S$ and metal dataset is lacking for the stratigraphy hosting Carlin-type deposits, and the $\delta^{34}S$ of sedimentary pyrite can vary widely depending on conditions. Studies have reported pyrite $\delta^{34}S$ values as light as −46 ‰ resulting from bacterial sulfate reduction (Kaplan and Rittenberg, 1964). Even in a single stratigraphic section, changes from open marine to closed basin conditions can cause major fluctuations in $\delta^{34}S$ values (e.g., −15 ‰ to +30 ‰; Johnson et al., 2018).

A comprehensive $\delta^{34}S$ and metal dataset would require systematic drilling, sampling, petrography, and geochemistry of unmineralized rocks from every stratigraphic unit hosting, underlying, and adjacent to Carlin-type mineralization. Although some stratigraphic intervals have been studied, the data are from within the deposit areas and may represent the epigenetic mineralizing events rather than the precursor stratigraphy. Furthermore, the low spatial resolution of existing standardized $\delta^{34}S$ data represents mixed signatures of precursor sedimentary sulfur and later Carlin-type hydrothermal pyrite. For example, Christiansen et al. (2010) collected 332 whole-rock $\delta^{34}S$ and Au analyses from the Devonian Popovich Formation in the Screamer zone of the Betze-Post deposit on the northern Carlin trend. Each data point represents a five-foot core interval, from holes drilled through high-grade zones and intervening low-grade and barren zones. The whole-rock $\delta^{34}S$ values range from −16.4 to 16.0 ‰. In intervals that assayed at higher Au grades, the $\delta^{34}S$ values are generally closer to zero. From these data it is impossible to precisely define the signature of the unmineralized host rocks, since there is no petrographic data documenting the presence or absence of Carlin-type hydrothermal pyrite overgrowths. Furthermore, the stratigraphy beneath and adjacent to the deposit remains uncharacterized. In one of our modeled scenarios, we included the $\delta^{34}S$ of unmineralized Popovich Formation stratigraphy from Christiansen et al. (2010), filtering the data to include only those sample intervals with gold assays below detection limit.

Other studies report a smaller number of conventional analyses of physical separates or leachates, generally suggesting a $\delta^{34}S$ range of −20 to 35 ‰ for diagenetic pyrite in northern Nevada (Hofstra and Cline, 2000; Kesler et al., 2003; Cline et al., 2005). However, the data lack petrographic context, so we cannot rule out contamination from the ore pyrite that commonly overgrows these grains. No studies have systematically examined all the non-pyrite sulfur-bearing phases in the stratigraphy, but Emsbo et al. (2003) analyzed separates of Late Devonian sedimentary exhalative and diagenetic barite, obtaining $\delta^{34}S$ values ranging from 22 to 52 ‰. Several studies have used traditional SIMS analyses to determine the $\delta^{34}S$ of individual pyrite grains or portions of those grains, but the analytical volume is large relative to the scale of the zonation in Carlin-type hydrothermal pyrite, and the results vary widely. Kesler et al. (2005) collected 22 traditional SIMS spots on pyrites from Screamer and reported that the cores gave $\delta^{34}S$ values of −0.9 to 3.6 ‰. Those authors did not analyze for gold, so it is unclear how many of the data points represent mixed analyses of diagenetic and hydrothermal pyrite. At Betze-Post, Henkelman (2004) reported a much wider range of traditional SIMS $\delta^{34}S$ values for pre-ore (presumably sedimentary) pyrite, from −15.2 to 52.3 ‰.

The NanoSIMS analyses of Carlin-type pyrite grain cores published in Holley et al. (2022) represent the highest spatial resolution standardized data available for sedimentary sulfur sources in the region, and we defined our local sedimentary source population based on these analyses. The data are from Au- and As-poor euhedral, framboidal, or porous sedimentary cores of grains from Getchell, Carlin, and Turquoise Ridge. These grains are rimmed by Au- and As-rich hydrothermal pyrite rims, and the rim data are included in the mixtures. The $\delta^{34}S$ values of the pyrite cores ranged from 20.3 to 54.4 ‰, suggestive of diagenesis of iron-poor, carbonaceous sediments in a closed marine basin. The Au concentrations of these zones ranged from below detection limit to 4.6 ppm. These sedimentary sources of sulfur and metals were already present in the stratigraphy during Eocene Carlin-type mineralization. We did not apply fractionation corrections to the sedimentary source data, since their contribution to the mineralizing fluids would have occurred via dissolution and stripping, and therefore no temperature-related fractionation is expected at the site of sulfur acquisition.

Table 1
Model configurations.

Model configuration	A: Two-source model	B: Three-source model	C: Three-source model
Mixtures	Hydrothermal pyrite rim $\delta^{34}S_{fluid}$ (NanoSIMS[a])	Hydrothermal pyrite rim $\delta^{34}S_{fluid}$ (NanoSIMS[a])	Hydrothermal pyrite rim $\delta^{34}S_{fluid}$ (NanoSIMS[a])
Source 1	Sedimentary pyrite $\delta^{34}S$ (NanoSIMS of grain cores[a])	Sedimentary pyrite $\delta^{34}S$ (NanoSIMS of grain cores[a])	Sedimentary pyrite $\delta^{34}S$ (NanoSIMS of grain cores[a])
Source 2	Eocene magmatic pyrite $\delta^{34}S_{fluid}$ (Eocene dike & hydrothermal sulfide minerals: NanoSIMS[a], whole-grain analyses[b])	Eocene magmatic pyrite $\delta^{34}S_{fluid}$ (Eocene dike & hydrothermal sulfide minerals: NanoSIMS[a], whole-grain analyses[b])	Eocene magmatic pyrite $\delta^{34}S_{fluid}$ (Eocene dike & hydrothermal sulfide minerals: NanoSIMS[a], whole-grain analyses[b])
Source 3	N/A	Jurassic & Cretaceous magma $\delta^{34}S$ (NanoSIMS of sulfide minerals[a] and whole-rock granitoid plutons[c])	Popovich Formation $\delta^{34}S$ (whole-rock[d])
Prior	Uninformative/ generalist	Uninformative/ generalist	Uninformative/ generalist
Mixture factors	Group	Group	Group
Source factors	NULL	NULL	NULL
Continuous effects	Au (ppm) of hydrothermal pyrite mixtures	Au (ppm) of hydrothermal pyrite mixtures	Au (ppm) of hydrothermal pyrite mixtures
Discrimination	0	0	0
Residual error	True	True	True
Process error	False	False	False
MCMC chain length	100,000	100,000	100,000

[a] Holley et al. (2022).
[b] Theodore et al. (1986) and King (2017).
[c] Arehart et al. (2013).
[d] Christiansen et al. (2010).

4.2.2. Older magmatic rocks

Jurassic and Cretaceous magmatic rocks occur throughout northern Nevada and were already present in the host rock package during Eocene Carlin-type mineralization. The intrusions and their magmatic-hydrothermal products potentially served as sources of metals and sulfur for Carlin-type ore. Known Jurassic units near Carlin-type districts include the Goldstrike stock (Arehart et al., 1993; Mortensen et al., 2000), as well as intrusions in the Cortez mountains (Stewart and McKee, 1977), Buffalo Mountain (Neff, 1973). Jurassic intrusions are also inferred in the Battle Mountain trend based on the presence of inherited zircon in Cretaceous intrusions (Fithian et al., 2018; Huff et al., in review). In some locations, such as at Goldstrike, the intrusions generated skarn mineralization in the hornfelsed aureole of the stock (Goldfarb et al., 2016). Cretaceous magmatic rocks include the Osgood stock near the Getchell trend (Groff et al., 1997), the Trenton Canyon stock and various dikes in the Battle Mountain district (Theodore et al., 1973; Theodore, 2000; Fithian et al., 2018; Huff et al., in review), and in the Carlin trend (Evans, 1980; Mortensen et al., 2000).

We used two sources of data to represent this possible contribution. Arehart et al. (2013) published a regional compilation of whole-rock sulfur isotopic data for granitoid plutons in the Great Basin, although trace metal concentrations are not included. The samples of known Jurassic age have whole-rock $\delta^{34}S$ values ranging from 0.6 to 17.5 ‰, and those that are known to be Cretaceous have whole-rock $\delta^{34}S$ values from −0.6 to 20.7 ‰ (Arehart et al., 2013). We also incorporated NanoSIMS and laser ablation multicollector ICPMS data from coarse magmatic-hydrothermal pyrites in the Jurassic skarn adjacent to the Goldstrike stock (Holley et al., 2022), with $\delta^{34}S$ values ranging from 6.5 to 6.9 ‰ and Au concentrations <0.1 ppm. Similar to the sedimentary source, no fractionation correction was applied to these data since older magmatic and magmatic-hydrothermal phases would have contributed to the Eocene mineralizing fluid via dissolution and stripping.

4.2.3. Eocene magmatic rocks

Although Eocene granitoid plutons occur throughout the Great Basin, Eocene intrusions are notable at some Carlin-type deposits but are either absent or remain unidentified at others. Eocene dikes have been intersected during exploration and mining in numerous deposits on the northern Carlin trend and have been well studied (Ressel and Henry, 2006). Holley et al. (2022) collected NanoSIMS $\delta^{34}S$ values of pyrite from three rock units previously dated by Ressel and Henry (2006) using $^{40}Ar/^{39}Ar$ methods: a devitrified high-silica aphyric rhyolite from Deep Star (39.15 ± 0.26 Ma; weighted mean of matrix), a finely porphyritic plagioclase-biotite ± quartz rhyolite from Betze Post (39.32 ± 0.11 Ma biotite), and the coarsely porphyritic plagioclase-biotite-hornblende-quartz ± sanidine Beast dike that hosted about half of the ore at the Beast deposit (37.58 ± 0.06 and 37.61 ± 0.06 Ma sanidine; 37.55 ± 0.07 Ma biotite). At Deep Star and Betze Post, the pyrite grains were lath shaped, trace element-poor, and lacked hydrothermal rims. At Beast, similar pyrite grains were encapsulated by fuzzy Carlin-type hydrothermal rims enriched in Au and As. We included the grain cores in the source dataset but reserved the hydrothermal rims for the mixture data set. The $\delta^{34}S$ values range from 7.9 to 15.2 ‰, with the lightest values from unmineralized euhedral pyrite grain cores at Beast. Arehart et al. (2013) obtained whole-rock $\delta^{34}S$ values from Tertiary plutonic rocks ranging from −3.2 to 20.2 ‰, with a mean of 7.1 ‰. We only included plutons that could have been actively generating fluids in the Eocene, so we could not include the data from Arehart et al. (2013) since exact ages of the intrusions were not reported.

The nearest significant Eocene mineralization of *proven* magmatic-hydrothermal origins occurred in the Battle Mountain district, 40 miles south of the Getchell trend and 60 miles west of the Carlin trend. Economic and subeconomic porphyry, skarn, and distal-disseminated deposits in the Battle Mountain district have been conclusively linked to Eocene magmatic systems (Theodore et al., 1973; Doebrich, 1995; Kizis et al., 1997; Meinert, 2000; Keeler, 2010; Reid et al., 2010; King, 2011; King, 2017; Holley et al., 2019). At the Eocene distal disseminated Lone Tree deposit, Holley et al. (2019) collected laser ablation multi-collector ICPMS $\delta^{34}S$ data from dike pyrite grain cores and Au-As-rich magmatic-hydrothermal rims. The grain cores have $\delta^{34}S$ values of 3.4 to 6.6 ‰ and Au concentrations below 0.4 ppm and are definitively of magmatic-hydrothermal origins, as evidenced by the δD and $\delta^{18}O$ values of sericite intergrowths. Theodore et al. (1986) and King (2017) reported the results of conventional whole-grain $\delta^{34}S$ analyses of Eocene porphyry and skarn sulfide minerals in the Battle Mountain district, including Buffalo Valley, Copper Basin, Copper Canyon, and Elder Creek. From this dataset we used the $\delta^{34}S$ values for chalcopyrite, galena, molybdenite, pyrite, pyrrhotite, and sphalerite, since the mineral-H_2S fractionations are well-established (Ohmoto and Rye, 1979; Li and Liu, 2006). For all the Battle Mountain district sulfide mineral data, we calculated the $\delta^{34}S$ compositions of the causative fluids at a range of realistic temperatures based on previously published descriptions of the sulfide paragenesis at each deposit (Appendix 1).

5. Modeling methods

We ran three configurations of the model to test the relationship between Au concentrations of the hydrothermal pyrites and the source contributions of $\delta^{34}S$ to those pyrites (Table 1). In Model A, we compared our mixture data points to two sources: 1) Sedimentary pyrite, represented by the composition of precursor grain cores of sedimentary origins in Carlin-type pyrite (Holley et al., 2022), and 2) Eocene magmatism, represented by the compositions of sulfide minerals from Carlin trend dikes and Battle Mountain magmatic-hydrothermal ore deposits (Theodore et al., 1986; King, 2017; Holley et al., 2022). In Model B, we added a third source: 3) Jurassic and Cretaceous magmatic rocks present in the region during Eocene mineralization, represented by whole rock plutonic sulfur from Great Basin granitoids (Arehart et al., 2013). In Model C, we used a different third source: 3) Unmineralized Popovich Formation rocks on the Carlin Trend (Christiansen et al., 2010). We attempted a 4-source model using all the sources described above, but that model was not solvable since the number of potential sources was significantly greater than the number of tracers. Last, we attempted a two-source model to determine whether the mixtures could be obtained only with contributions from the Sedimentary pyrite and the Popovich Formation sources. Significantly, the model was not solvable without a magmatic source.

In all model configurations, we set the Au concentration of the mixtures as a continuous effect, enabling examination of Au covariance with source contributions. We also divided our mixture data points into five groups, based on the five different ore deposits from which the samples were obtained. Model configurations A, B, and C converged using "normal" Markov Chain Monte Carlo chain lengths of 100,000, with diagnostics and summary statistics that are reasonably robust given the limited number of samples per deposit (Appendices 2 and 3). The other possible model settings such as discrimination (trophic enrichment factors) and prior knowledge of source contributions are not relevant for the case study. For a full description of all model settings designed for ecological studies, see Stock (2022). The codes for the model are provided in Appendix 4.

6. Results

6.1. Model A

The plots produced by MixSIAR enable visualization of the probability distributions of Eocene magmatic and sedimentary source contributions during Carlin-type mineralization (Fig. 3). For the combined dataset of all the hydrothermal pyrite, there is a high probability that the contribution of sulfur from Eocene magmatism is greater than the contribution from the sedimentary pyrite (Fig. 3a,b). This supports the interpretations reached by Holley et al. (2022) based on the raw data.

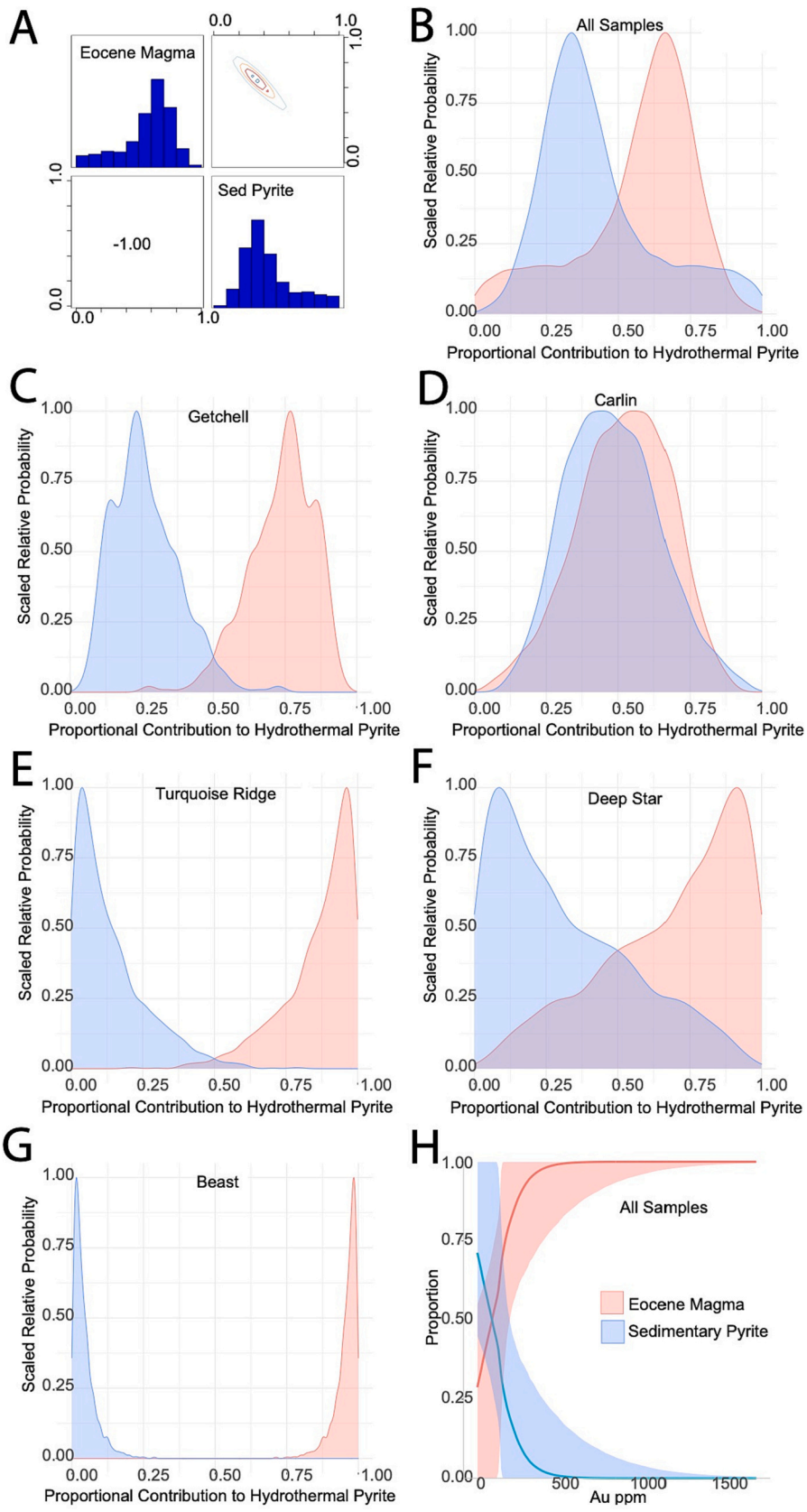

Fig. 3. Two-source MixSIAR Model A showing probability distributions for Eocene magmatic and local sedimentary pyrite contributions of $\delta^{34}S$ to the hydrothermal pyrite. (A) Matrix plot of sources; histograms indicate probability distributions for each of the sources; numeric value −1.00 is correlations between contributions of the two sources; contour diagram shows the joint probability of both sources. Scaled relative probability (y-axis) of proportional source contribution (x-axis) for (B) All sample analyses, and analyses from (C) Getchell, (D) Carlin, (E) Turquoise Ridge, (F) Deep Star, and (G) Beast. (H) Proportional source contribution covaries with Au concentration; lines within the shaded regions show the posterior median estimates of the slope and intercept. (For interpretation of the references to colour in this figure legend, the reader is referred to the web version of this article.)

The contributions of the two sources show trends inverse to one another, which is tautological for a two-source model. When we assess the hydrothermal pyrite mixtures based on the deposits from which the grains were sampled, there is considerable variation in proportional source contribution among deposits (Fig. 3c–g). At Getchell (Fig. 3c), Turquoise Ridge (Fig. 3e), and Beast (Fig. 3g), the Eocene magmatic sulfur contribution is likely much higher than the contribution of sulfur from the sedimentary pyrite. At Carlin, the relative proportions are roughly equal (Fig. 3d). At Deep Star there is only one mixture data point, and the model results indicate that nearly all the sulfur was most likely derived from magmas, but all relative proportions are possible (Fig. 3f). For the combined dataset from all five deposits, the modeled covariance between Au and source contribution shows that the proportion of Eocene magmatic sulfur is positively correlated with Au concentration of the hydrothermal pyrite: the nanoscale hydrothermal pyrite zones with high Au most likely derived all of their sulfur from Eocene magmas (Fig. 3h).

6.2. Model B

Model B compares the contributions of Eocene magmatism, sedimentary pyrite grain cores, and Cretaceous and Jurassic magmatic rocks that were present in the region during Eocene mineralization. For the combined dataset of all the Carlin-type hydrothermal pyrite, there is low probability of major contributions from sedimentary pyrite or the pre-existing Jurassic and Cretaceous magmatic rocks (Fig. 4a). When we examine the hydrothermal pyrites grouped by deposit, the results corroborate the two-source model, suggesting that Eocene magmas likely contributed the majority of sulfur at Getchell (Fig. 4b), Turquoise Ridge (Fig. 4d), and Beast (Fig. 4f). At these locations, the modeled contributions of sedimentary pyrite are similar to those of the older Jurassic and Cretaceous magmatic sulfur. At Carlin, the contributions of the Eocene magmas and sedimentary pyrite are non-differentiable from one another, as in the two-source model, and it is most likely that the sulfur contributions from Jurassic and Cretaceous magmatic rocks were small (Fig. 4c). Like the two-source model, the Model B results suggest that most of the sulfur in the Carlin-type pyrite at Deep Star came from Eocene magmas, although all combinations are possible (Fig. 4e). The Au covariate plot for Model B shows that as Au concentrations increase in the hydrothermal pyrite, the contributions of sedimentary pyrite and preexisting Jurassic and Cretaceous magmatic rocks decrease, whereas the contributions of Eocene magmas increase (Fig. 4g).

6.3. Model C

Model C compares the contributions of Eocene magmatism, sedimentary pyrite grain cores, and unmineralized Popovich Formation stratigraphy present on the Carlin trend. Combined analyses of all the hydrothermal pyrites shows that the relative contributions of the Popovich Formation are low (Fig. 5a, b) and vary inversely with Au concentration. We show an example from the Carlin deposit: the contributions of local sedimentary pyrite decrease with Au concentration, whereas the potential contributions of Popovich Formation stratigraphy and Eocene magmas increase with Au concentration (Fig. 5c–f). As discussed in the section on Model Inputs, it is impossible to fully constrain the contributions of the sedimentary rock package, and the Popovich Formation is the most poorly defined of all the potential sources in our model. Despite this uncertainty, we observe the same trend of increasing contribution from Eocene magmas with increasing Au concentrations in the hydrothermal pyrite.

7. Discussion

7.1. Modeled origins of Carlin-type gold

Our MixSIAR modeling of the sulfur source contributions to the hydrothermal pyrite can be used to infer the likely sources of the gold, since the gold and sulfur traveled together as bisulfide complexes during Carlin-type mineralization (Cline et al., 2005). Multiple potential sources of sulfur and gold existed in the region during mineralization, including Eocene magmas, older Jurassic and Cretaceous magmatic rocks, sedimentary rocks in the stratigraphy hosting the ore, and the precursor pyrite onto which the hydrothermal pyrite formed. The MixSIAR modeling revealed five key points:

First, multiple sources contributed to Carlin-type hydrothermal pyrite during fluid mixing. Numerous scholars have debated whether Carlin-type gold was sourced from magmatic fluids (Sillitoe and Bonham, 1990; Henry and Boden, 1998; Ressel et al., 2000; Johnston and Ressel, 2004; Seedorff and Barton, 2004; Muntean et al., 2011), or from circulating meteoric or metamorphic fluids (Hofstra, 1994, 1995; 1999; Ilchik and Barton, 1997; Emsbo et al., 1999, 2003; Hofstra and Cline, 2000; Large et al., 2011). All four of our modeled sources likely contributed to hydrothermal Carlin-type pyrite, and no single source can explain the variance among deposits and within grains, suggesting that deposit genesis probably involved aspects of both proposed processes.

Second, the compositions of the hydrothermal pyrite cannot be achieved without a magmatic source. Large et al. (2011) proposed that the gold was already present in the sedimentary host rocks, trapped in diagenetic pyrite and organic matter. In the rocks hosting most of the gold on the Carlin trend, the mean background concentrations of gold and arsenic are 15 and 25 times the crustal averages, respectively; for example, unmineralized rocks of the Popovich Formation contain a mean of 28 ppb Au (Large et al., 2011). Large et al. (2011) proposed that structural deformation or intrusive activity initiated the lateral movement of meteoric fluids through the carbonaceous sedimentary rocks. These meteoric fluids “stripped” the gold and arsenic and then redeposited the metals onto precursor diagenetic pyrite grains in lithologically or structurally favorable host rocks. Although the modeling shows that the sedimentary host rocks contributed sulfur to the hydrothermal pyrite, the mixing model cannot be solved using only sedimentary sources. This resonates with first-order observations on the geology of Northern Nevada. The region experienced major periods of magmatism in the Jurassic, the Late Cretaceous, and the Eocene, resulting in a metasomatized and potentially metal-rich sub-continental lithospheric mantle (Muntean et al., 2011). Given the occurrence of intrusions of various ages near many Carlin-type deposits, as a matter of course some magmatic sulfur would have made its way into the hydrothermal fluid during mineralization, regardless of the mechanism and timing.

Third, Eocene magmas contributed to hydrothermal pyrite growth, even in deposits where proximal Eocene intrusions are not known. The modeling indicates an Eocene magmatic contribution at Carlin, Deep Star, and Beast on the Carlin Trend, where geochronology of dikes and airborne magnetic surveys have been used to infer the presence of an underlying ~12 × 50 km Eocene composite batholith (Ressel and Henry, 2006). The modeling also indicates that Eocene magmas contributed to hydrothermal pyrite at Turquoise Ridge and Getchell where no Eocene intrusions are known; the nearest documented Eocene magmatic rocks are dacite tuffs approximately four miles north of Chimney Creek (Cline et al., 2005). Based on this evidence, we suggest that Eocene magmatic fluids were also circulating during mineralization in other Carlin-type districts where no Eocene magmatic rocks have yet been identified.

Given that Carlin-type mineralization is thought to be Eocene at locations where dating has been achieved, we infer that the hydrothermal pyrites grew in the magmatic-hydrothermal environment during Eocene magmatism, rather than deriving their Eocene component through amagmatic fluid circulation and stripping of existing Eocene magmatic rocks. At most Carlin-type deposits, an Eocene age for mineralization has been inferred based on crosscutting relationships (numerous studies compiled in Cline et al., 2005; Ressel and Henry, 2006). Direct dating has only occurred at only a few deposits: Eocene ages were obtained at Getchell adjacent to Turquoise Ridge using Rb-Sr dating of late ore-stage galkhaite (a rare Hg-sulfosalt; Tretbar et al., 2000; Arehart et al., 2003)

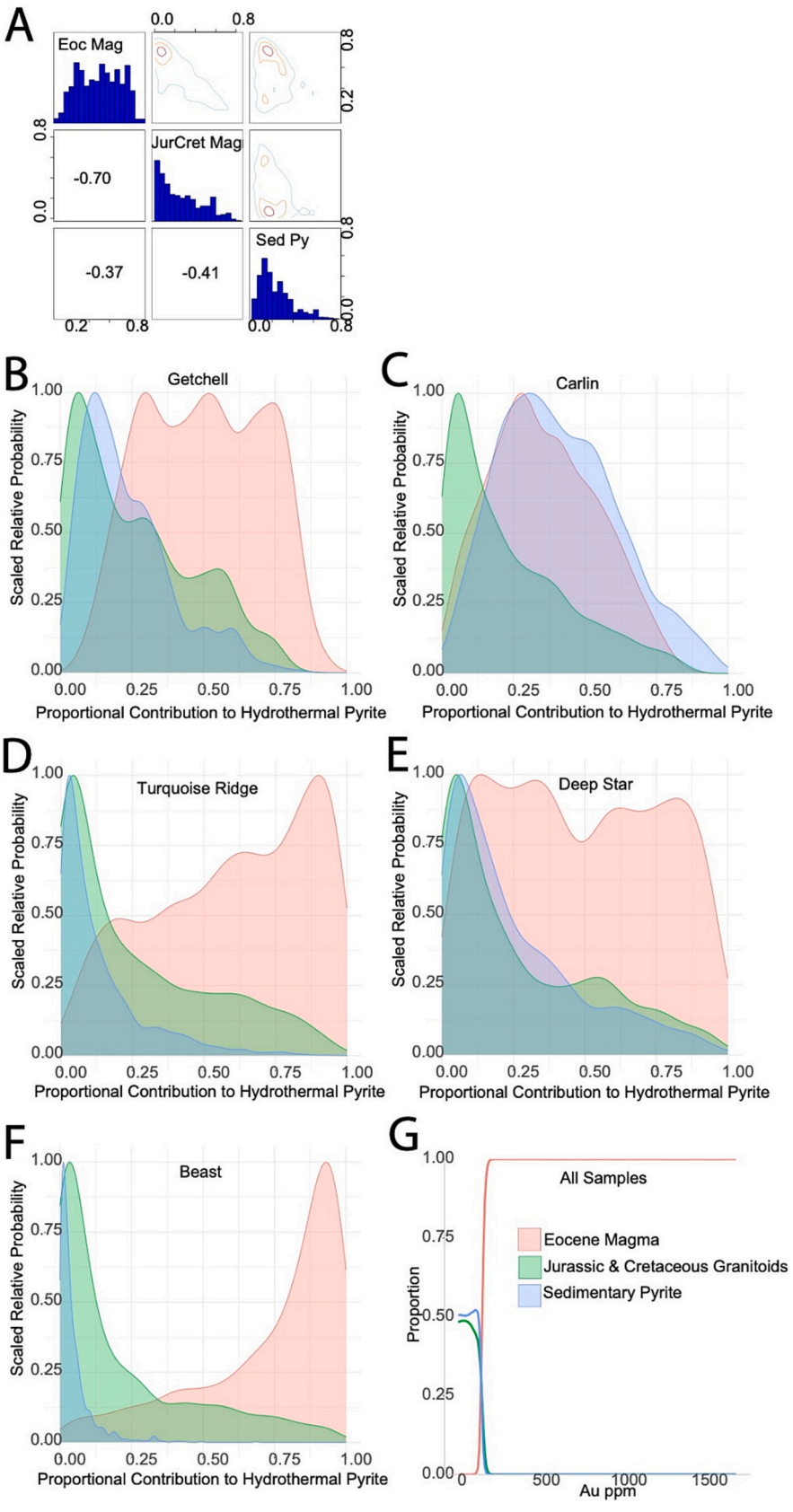

Fig. 4. Three-source MixSIAR Model B showing probability distributions for Eocene magmatic, Jurassic and Cretaceous granitoid, and local sedimentary pyrite contributions of $\delta^{34}S$ to the hydrothermal pyrite. (A) Matrix plot of sources; histograms indicate probability distributions for each of the sources; numeric values in the cells are correlations between contributions of pairs; contour diagrams show joint probabilities of pairs. Scaled relative probability (y-axis) of proportional source contribution (x-axis) for (B) Getchell, (C) Carlin, (D) Turquoise Ridge, (E) Deep Star, and (F) Beast. (G) Proportional source contribution covaries with Au concentration; lines show the posterior median estimates of the slope and intercept. (For interpretation of the references to colour in this figure legend, the reader is referred to the web version of this article.)

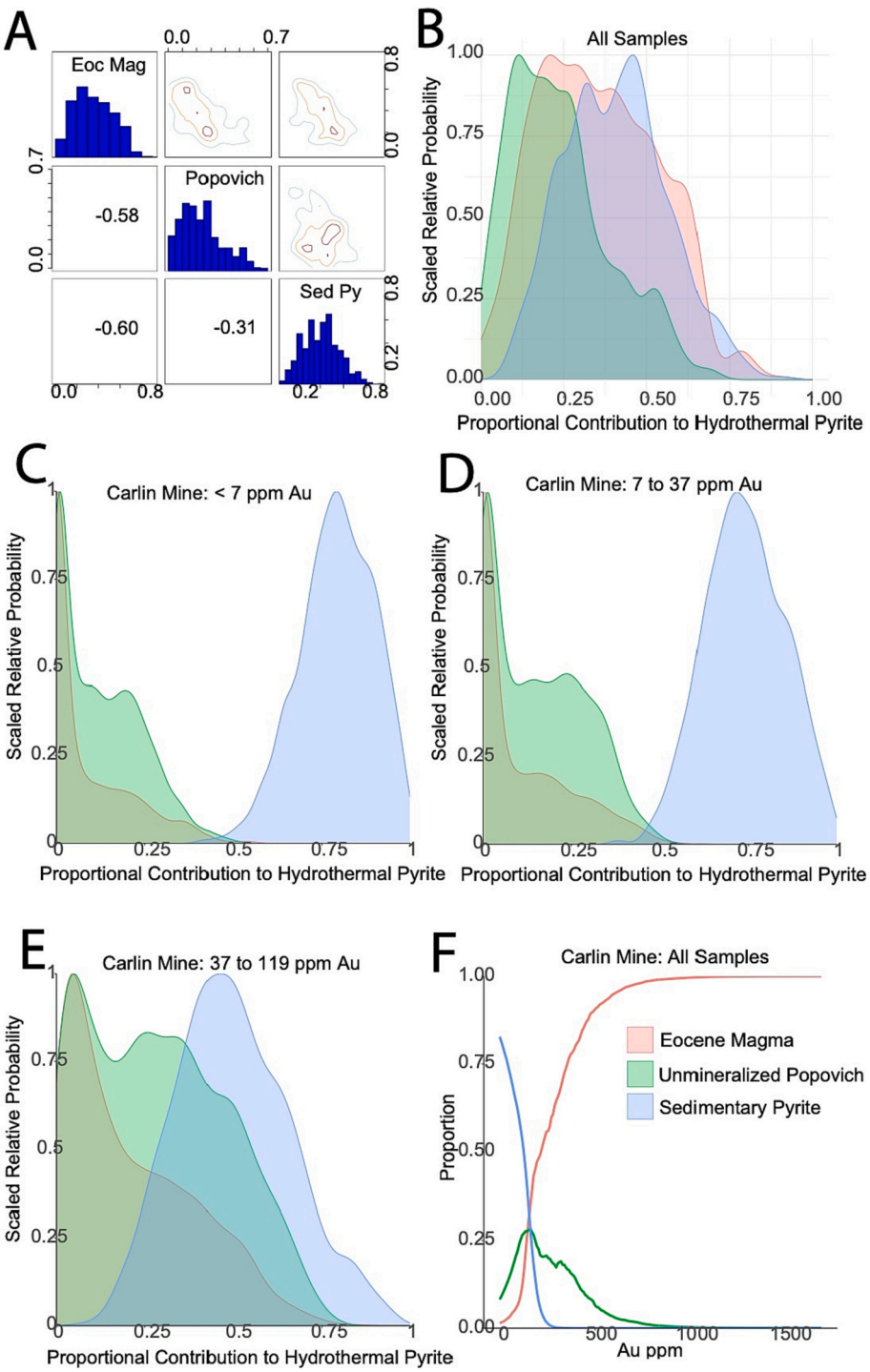

Fig. 5. Three-source MixSIAR Model C showing probability distributions for Eocene magmatic, unmineralized Popovich Formation, and local sedimentary pyrite contributions of $\delta^{34}S$ to the hydrothermal pyrite. (A) Matrix plot of sources; histograms indicate probability distributions for each of the sources; numeric values in the cells are correlations between contributions of pairs; contour diagrams show joint probabilities of pairs. Scaled relative probability (y-axis) of proportional source contribution (x-axis) for (B) All samples, (C) Carlin mine analyses with low Au, (D) Carlin mine analyses with moderate Au, and (E) Carlin mine analyses with high Au. (F) Proportional source contribution in the Carlin analyses covaries with Au concentration; lines show the posterior median estimates of the slope and intercept.

and Ar-Ar dating of adularia at Twin Creeks on the Getchell Trend (Groff et al., 1997; Hall et al., 1997). The adularia was sampled from vein mineralization atypical of Carlin-type mineralization and the paragenetic relationship with gold is not entirely certain. Apatite fission track and apatite (U-Th)/He ages are reset by the temperature and duration of Carlin-type mineralization and have been used to obtain evidence for a pulse of late Eocene hydrothermal fluid flow on the Carlin trend (Arehart et al., 1993; Chakurian et al., 2003; Arehart et al., 2003; Hickey et al., n.d.), the Getchell trend, (one sample; Hofstra et al., 1999), and at numerous sedimentary rock hosted gold deposits in the Battle Mountain district (Huff et al., in review). While further studies are needed to refine the timing of magmatism and mineralization throughout the region, we interpret the available data to mean that the Eocene magmatic contribution to the hydrothermal pyrite occurred via magmatic-hydrothermal processes contemporaneous with mineralization.

Fourth, the modeled covariance between Au and $\delta^{34}S$ indicates that Eocene magmas were the source of high-Au zones in Carlin-type pyrite. Although it is possible that metalliferous horizons in the sedimentary rock contributed some gold during hydrothermal pyrite growth (e.g., Emsbo et al., 2003; Large et al., 2011), our modeling shows that the Au-rich zones are mostly derived from Eocene magmatic sources. We envision a metal-rich magma similar to that described by Muntean et al. (2011). Those authors determined that emplacement of this hydrous,

calc-alkaline magma of intermediate composition at 10 to 12 km depth would lead to exsolution of a single-phase, metal- and H_2S-rich aqueous fluid. Phase separation would condense out a small quantity of hypersaline liquid into which the Fe, Ag, and base metals would partition. The ascending vapor phase would transport Au, As, Sb, and S into the shallow crust, consistent with evidence for magmatic-hydrothermal formation of porphyry and epithermal ores (Heinrich, 2005). We infer that the majority of the Au in Carlin-type pyrite was derived from this type of fluid.

Finally, mixing was essential to generate the observed compositions of the hydrothermal pyrite, and the proportional source contributions varied over space and time.

The hydrothermal pyrites are the product of mixing between multiple fluids, and the intra-grain spatial zonation of the individual grains require that the relative contributions of fluid sources varied over time during growth of the hydrothermal pyrite. Inter-deposit compositional heterogeneities suggest that the mixing occurred locally rather than regionally. Intra-grain and inter-grain within individual deposits further indicate that mixing was local.

Other evidence in the literature supports our interpretation of local fluid mixing. The geochemical signatures of ore-stage alteration minerals vary in Carlin-type deposits (Cline et al., 2005); at Deep Star for example the $\delta^{18}O$ and δD of ore-stage kaolinite suggest mixing of magmatic and meteoric fluids (Heitt et al., 2003; Cline et al., 2005). At the Getchell deposit, the isotopic compositions of fluid inclusions in ore-stage quartz and late ore-stage calcite show a mixing trend between magmatic (or metamorphic) and exchanged meteoric fluids (Hofstra and Cline, 2000). Furthermore, we suggest that the ambiguity in sulfur source for previously published studies of $\delta^{34}S$ in Carlin-type pyrite (Cline et al., 2003; Kesler et al., 2003; Henkelman, 2004; Cline et al., 2005; Kesler et al., 2005; Barker et al., 2009) may be representative of local mixing that could not be resolved for quantified in the absence of a suitable modeling technique.

In the genetic model proposed by Muntean et al. (2011), gold in the magmatic-hydrothermal fluid would have precipitated on precursor pyrite grains in the host rock, in association with cooling due to ascent and entrainment of meteoric water. Here we invoke mixing with the meteoric fluid proposed by Large et al. (2011), although our modeling indicates that it carried little of the gold. Local mixing of magmatic-hydrothermal (Muntean et al., 2011) and meteoric (Large et al., 2011) fluids led to pyrite precipitation. Episodic flux in proportional contributions resulted in geochemical zonation within the hydrothermal pyrite, as well as intra- and inter-deposit heterogeneity.

7.2. Assessment of the modeling approach

Bayesian mixing models are a statistically robust approach to quantitatively solve geochemical mixing problems, relative to qualitative approaches common in interpretations of ore deposit genesis, and relative to the non-Bayesian mixing models previously used in ecological studies (e.g., IsoError, IsoSource). Table 2 compares the main features and capabilities of these methods. The Bayesian models such as MixSIAR are the most sophisticated approach available for solving mixing problems. This class of model is ideally suited to solve geochemical problems in the field of ore deposits, since such models can incorporate variance in source mixture populations, are suitable for underdetermined systems with more potential sources than tracers, and can assess the variation of source proportions with a continuous covariate such as trace element concentration. However, this class of model is less user-friendly than alternative approaches, requiring a deeper understanding of statistics and at least a basic level of proficiency in the R environment for statistical computing.

Table 2
Comparison of methods for single-tracer ($\delta^{34}S$) analyses of Carlin-type pyrite.

	Qualitative	IsoError	IsoSource	MixSIAR
Number of sources	2	2	2–4	2–4
Source characterization	Raw data	Mean, SD	Mean	Raw data
Covariation (with Au)	Yes	No	No	Yes
Computer platform	N/A	Excel	Visual basic	R
User effort	Low	Low	Low	Higher
Statistical robustness	Low	Low	Low	High

For comparison to the MixSIAR modeling, we conducted a simple qualitative assessment of the $\delta^{34}S$ and Au data used in this study. For each ore deposit, the individual pyrite analyses plot on a mixing trend between the sedimentary pyrite and a composition similar to that of Eocene magmatic fluids (Fig. 6a–c). Similarly, for whole-rock analyses the $\delta^{34}S$ appears to vary with Au concentration, approaching the composition of Eocene magmatic fluids as Au increases (Fig. 6d). The observed mixing is consistent with the outcomes from our MixSIAR modeling. However, MixSIAR allows for more nuanced observations on the proportional source contributions, as well as modeling of more than two sources.

IsoError (Phillips and Gregg, 2001a, 2001b) only allows modeling of two sources with a single isotopic tracer, although three sources can be modeled if there are two tracers. The source and mixture populations are represented by means and standard deviations rather than the raw values. We used IsoError to calculate two-source mixing models for the same dataset (Appendix 1), and the results (Fig. 6e) were mostly consistent with our MixSIAR modeling. Models including Eocene magmas and the sedimentary pyrite require contributions from both the magmatic and the sedimentary sources. Unlike the MixSIAR models, the results from IsoError suggest that the mixture population can be explained with contributions from older magmatism and local sedimentary pyrite, or with only sedimentary sources. These results could lead to spurious conclusions since they only draw on means and standard deviations; modeling the raw data in MixSIAR shows that the mixtures cannot be explained without a magmatic source contribution.

Although IsoSource (Phillips and Gregg, 2003) can be used in underdetermined systems, it only allows for input of means or single values to represent a population, without addressing variance of the populations. We ran a 4-source model (Fig. 6f) using the means for the mixtures and the means for the sources from the MixSIAR modeling (Appendix 1). Using an increment of 1 % for possible contributions to the mixture's mean, the model requires a non-zero Eocene magmatic contribution in 97 % of all solutions. However, the contribution of Eocene magmas is generally a relatively small percentage of the total, ranging from 0 to 61 % for the Eocene magmas (mean of 19 %). Feasible contributions range from 33 to 48 % for the local sedimentary pyrite (mean of 41 %), from 0 to 58 % for the Popovich Formation (mean of 18 %), and from 0 to 67 % for Jurassic and Cretaceous magmas (mean of 21 %). Since IsoSource operates without consideration of variance, it does not facilitate exploration of the effects of heterogeneity within source or mixture populations. We find the IsoSource results insufficiently nuanced, since the most interesting aspect of the Carlin dataset is the covariance of the hydrothermal pyrite mixture $\delta^{34}S$ data with Au concentration.

Despite the advantages of Bayesian mixing models such as MixSIAR, there are limitations to the approach, some of which are inherent to any mixing model. For example, only the source contributions from *known* source populations can be modeled. In our case study, the modeling of Carlin-type pyrite may not account for all potential sources, since it is infeasible to quantify the sulfur isotopic signatures of the entire rock package within, above, below, and adjacent to Carlin-type deposits. The same limitation applies to ecological studies, where it is not realistic to track every single potential source in a consumer's diet. Furthermore, although MixSIAR is designed to be used in underdetermined systems (in which the number of potential sources exceeds the number of tracers by one or more), the results become less robust as the number of sources increases. In our case we must rely on Occam's razor: the mixture population can be fully explained by simple two- or three-source mixtures,

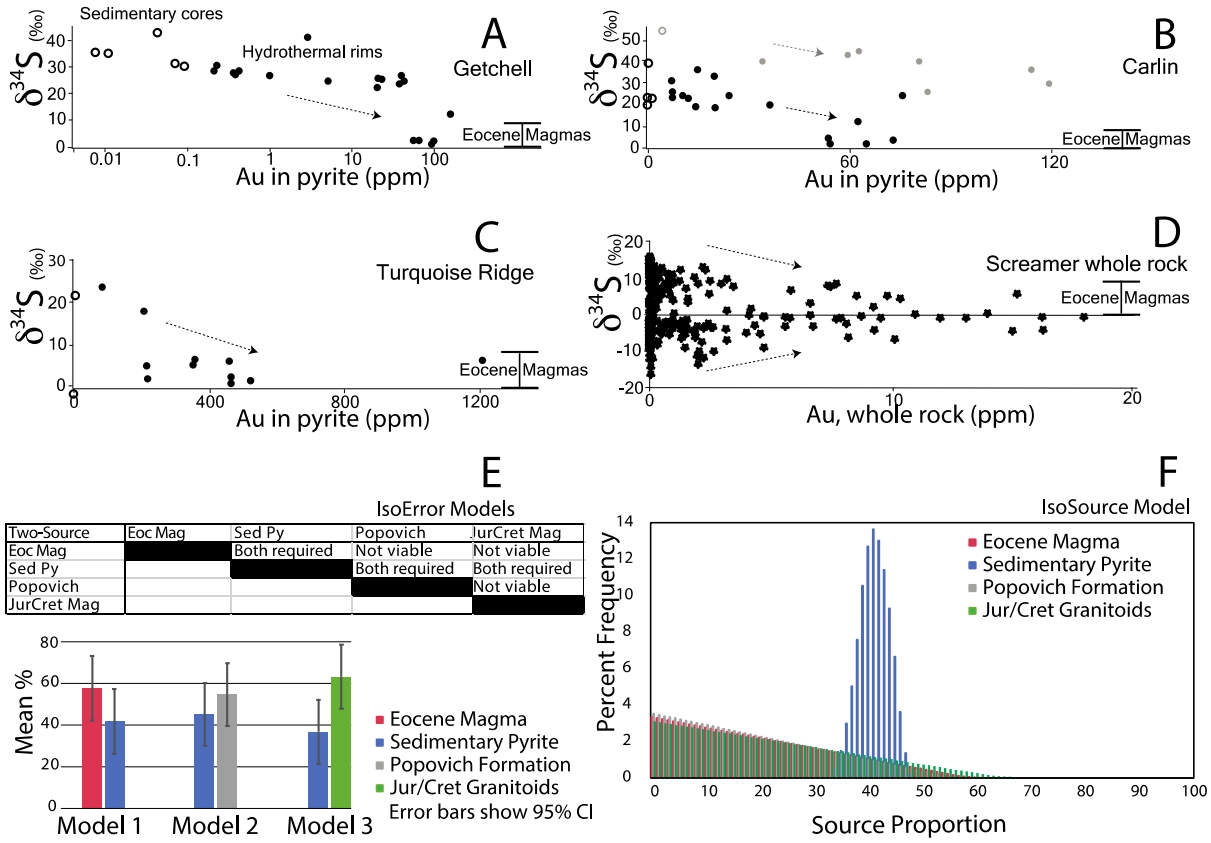

Fig. 6. Comparison to other methods. The dashed arrows in (A)–(D) show qualitative trends observed for covariation between $\delta^{34}S$ and Au, suggesting mixing between sedimentary pyrite (low Au datapoints near the Y-axis) and Eocene magmatic fluids (range shown with whisker symbol). (A)–(C) are NanoSIMS data (Holley et al., 2022), and the black and gray symbols in B show two different samples. (D) shows whole-rock analyses (Christiansen et al., 2010), and the direction of covariation is opposite for positive and negative $\delta^{34}S$ values. (E) IsoError two-source models using population means and standard deviations. (F) IsoSource four-source model using only population means; with the exception of the sedimentary pyrite, the trends for the other three sources are nearly identical.

with a clear trend of covariance between Au concentrations and Eocene magmatic source contributions.

Like any modeling method, the mixing results given by MixSIAR are only as valid as the input data. We acknowledge that the input data for the sedimentary sulfur sources are particularly problematic, since the $\delta^{34}S$ of sedimentary pyrite, organosulfur complexes, and other sulfur minerals in sedimentary rocks can vary widely. Secondly, the range of our Jurassic and Cretaceous magmatic source may have been unnecessarily wide, since the sample locations for the dataset spanned the Great Basin. More robust conclusions could be drawn on the contributions of these rocks if the range were restricted to those units located near Carlin-type deposits. Overlapping ranges of the source populations may be unavoidable for geologic units of similar origins, such as the Eocene and older magmatic sulfur. Another potential limitation is that the MixSIAR modeling method does not allow for the uncertainty associated with individual datapoints, although population-level standard deviations are an input if the user elects to use population means rather than raw data. In Appendix 1 we provide the standard deviation (ratio error) for each of our $\delta^{34}S$ mixture and source datapoints. Given the range of analytical techniques used by previous authors during collection of the original $\delta^{34}S$ data, the uncertainties vary within the dataset. Further studies should explore the sensitivity of the modeled results to the analytical uncertainties in the input data, and future advancements in the MixSIAR framework should incorporate uncertainties in the raw data. In contrast to the $\delta^{34}S$ data, the Au data for the mixtures (Appendix 1) were collected using a consistent method for the entire dataset. The relative sensitivity factor method (Zhang et al., 2017) that Holley et al. (2022) used to calibrate the Au concentrations is internally consistent, so even if there were inaccuracies in the absolute values, the relative Au concentrations would not vary. Since these relative values are the basis of the covariance calculations, we interpret the modeled results to be insensitive to uncertainty.

Many ore deposit studies only include data from a single isotopic system, so in some situations, trace element data may be used in a Bayesian tracer model in addition to stable isotopes. Caution must be taken to ensure that all tracers record the geological processes under investigation, rather than other older or overprinting events. As in the case of the Carlin study, it is rare to have access to trace element data and isotopic data that represent the same spatial resolution for all relevant sources as well as the mixture. Since minerals and ore deposits are commonly spatially zoned, it is important to ensure that data are of equivalent scale if multiple tracers are employed.

An advantage of Bayesian tracer modeling is that the approach is agnostic to the type of input data. The method can be used in the total absence of stable isotope data, as in the case of stream sediment geochemical datasets. The trace elements can be used as tracers in lieu of stable isotopes, and the modeling can help identify the proportional tributary contributions to a downstream sample. A deconvolutional component of MixSIAR has been developed for sediment source apportionment (Blake et al., 2018), and this could be adapted to account for the structural hierarchy of stream sediment exploration geochemistry samples in a watershed.

8. Conclusions

Bayesian mixing models can be useful to decipher source contributions in ore deposit geochemistry, as demonstrated in the example of Carlin-type pyrite. Using MixSIAR, we were able to show that multiple

sources contributed to Carlin-type pyrite during fluid mixing, but that the observed $\delta^{34}S$ compositions cannot be achieved without a magmatic contribution. The MixSIAR modeling shows that Eocene magmas contributed to the hydrothermal pyrite even in deposits where proximal Eocene intrusions are not known. Furthermore, the modeled covariance between Au and $\delta^{34}S$ suggests that the high-Au zones in the hydrothermal pyrite were sourced from Eocene magmas. Lastly, since the composition of the hydrothermal pyrite varies within grains, the MixSIAR modeling shows the possible range of source contributions necessary to achieve this observed variation. Overall, the modeling provides a statistically robust assessment of the two main theories for Carlin-type deposit formation, showing that both magmatic and meteoric fluids were important during mineralization.

Bayesian tracer models such as MixSIAR have both strengths and limitations that impact their utility in assessing the source contributions to mineralization. Like any modeling method, the results are only as valid as the input data. Since it is difficult to fully define all the possible source contributors to any mineralizing system, interpretations rely to some extent on Occam's razor to identify the simplest solution to the mixing problem. Relative to qualitative observations of mixing, or simpler quantitative mixing models such as IsoError and IsoSource, MixSIAR is better suited for underdetermined systems and populations with internal variance. The method is agnostic to tracer types and can be used with trace element or stable isotope data. Beyond studies of ore deposit geochemistry, we further suggest that Bayesian mixing models have other useful applications in geology, including study of oil type mixing in petroleum systems, sediment provenance, geochronology of mixed age populations, and magma mixing.

CRediT authorship contribution statement

E.A.H. and D.L.P. conducted the modeling.
E.A.H. wrote the manuscript and drafted the figs.
D.L.P. reviewed the manuscript and figures.

Declaration of competing interest

The authors declare no competing interests.

Acknowledgements

This study was funded by U.S. National Science Foundation (NSF) Career Award EAR-1752756 (E.A. Holley). We thank Al Hofstra, Christie Jilly-Rehak, Craig Johnson, Mike Pribil, and Mike Ressel for helpful discussions on the input data, and Brian Stock for advice on the modeling.

Appendices. Supplementary data

Supplementary data to this article can be found online at https://doi.org/10.1016/j.gexplo.2022.107091.

References

Arehart, G.B., Foland, K.A., Naeser, C.W., Kesler, S.E., 1993. 40 Ar/ 39 Ar, K/Ar, and fission track geochronology of sediment-hosted disseminated gold deposits at Post-Betze, Carlin Trend, northeastern Nevada. Econ. Geol. 88, 622–646.
Arehart, G.B., Chakurian, A.M., Tretbar, D.R., Christensen, J.N., McInnes, B.A., Donelick, R.A., 2003. Evaluation of radioisotope dating of Carlin-type deposits in the Great Basin, western North America, and implications for deposit genesis. Econ. Geol. 98, 235–248.
Arehart, G.B., DeYoung, S., Poulson, S.R., Heaton, J.S., Weiss, S., 2013. Sulfur isotopes in plutonic rocks of the Great Basin as indicators of crustal architecture. J. Geol. 121 (4), 355–369.
Barker, S.L.L., Hickey, K.A., Cline, J.S., Dipple, G.M., Kilburn, M.R., Vaughan, J.R., Longo, A.A., 2009. Uncloaking invisible gold: use of NanoSIMS to evaluate gold, trace elemnts, and sulfur isotopes in pyrite from Carlin-type gold deposits. Econ. Geol. 104, 897–904.
Blake, W.H., et al., 2018. A deconvolutional Bayesian mixing model approach for river basin sediment source apportionment. Sci. Rep. 8, 13073.
Bonham-Carter, G.F., Goodfellow, W.D., 1986. Background corrections to stream sediment geochemical data using digitized drainage and geological maps: application to Selwyn Basin, Yukon and Northwest Territories. J. Geochem. Explor. 25, 139–155.
Bonham-Carter, G.F., Rogers, P.J., Ellwood, D.J., 1987. Catchment basin analysis applied to surficial geochemical data, Cobequid Highlands, Nova Scotia. J. Geochem. Explor. 29, 259–278.
Carranza, E.J.M., 2009. Catchment basin analysis of stream sediment anomalies. In: Hale, M. (Ed.), Handbook of Exploration and Environmental Geochemistry.
Carranza, E.J.M., Hale, M., 1997. A catchment basin approach to the analysis of reconnaissance geochemical-geological data from Albay Province, Philippines. J. Geochem. Explor. 60, 157–171.
Chakurian, A.M., Arehart, G.G., Donelick, R.A., Zhang, X., Reiners, P.W., 2003. Timing constraints of gold mineralization along the Carlin trend utilizing apatite fission-track, 40Ar/39Ar, and apatite (U-Th)/He. Econ. Geol. 98, 1159–1171.
Christiansen, W.D., Hofstra, A.H., Zohar, P.B., Tousignant, G., 2010. Geochemical and stable isotopic data on barren and mineralized drill core in the Devonian Popovich Formation, Screamer sector of the Betze-Post gold deposit, northern Carlin trend, Nevada (No. 2010-1077). In: U.S. Geological Survey Open-File Report 2010-1077, 11p.
Cline, J.S., Hofstra, A.H., Muntean, J.L., Tosdal, R.M., Hickey, K.A., 2005. Carlin-type gold deposits in Nevada: critical geologic characteristics and viable models. In: Economic Geology 100th Anniversary Volume, 451, p. 484.
Cline, J.S., Stuart, F.M., Hofstra, A.H., Premo, W., Riciputi, L., Tosdal, R.M., Tretbar, D. R., 2003. Multiple sources of ore-fluid components at the Getchell Carlin-type gold deposit, Nevada, USA. In: Eliopoulos, D., et al. (Eds.), Mineral exploration and sustainable development: Rotterdam, Millpress, 2, pp. 265–268.
Doebrich, J.L., 1995. Geology and mineral deposits of the Antler Peak 7.5-minute quadrangle, Lander County, Nevada. In: Nevada Bureau of Mines and Geology Bulletin, 109, 44 p.
Ellison, A.M., 2004. Bayesian inference in ecology. Ecol. Lett. 7, 509–520.
Emsbo, P., Hutchinson, R.W., Hofstra, A.H., Volk, J.A., Bettles, K.H., Baschuck, G.J., Johnson, C.A., 1999. Syngenetic Au on the Carlin trend: implications for Carlin-type deposits. Geology 27, 59–62.
Emsbo, P., Hofstra, A.H., Lauha, E.A., Griffin, G.L., Hutchinson, R.W., 2003. Origin of high-grade gold ore, source of ore fluid components, and genesis of the Meikle and neighboring Carlin-type deposits, northern Carlin trend, Nevada. Econ. Geol. 98 (6), 1069–1105.
Evans, J.G., 1980. Geology of the Rodeo Creek NE and Welches Canyon quadrangles, Eureka County, Nevada, U.S. Geological Survey Bulletin 1472, 81 p.
Fithian, M.T., Holley, E.A., Kelly, N.M., 2018. Geology of gold deposits at the Marigold mine, Battle Mountain district, Nevada. Rev. Econ. Geol. 20, 121–155.
Francis, T.B., Schindler, D.E., Holtgrieve, G.W., Larson, E.R., Scheuerell, M.D., Semmens, B.X., Ward, E.J., 2011. Habitat structure determines resource use by zooplankton in temperate lakes. Ecol. Lett. 14, 364–372.
Fusswinkel, T., Wagner, T., Wälle, M., Wenzel, T., Heinrich, C.A., Markl, G., 2013. Fluid mixing forms basement-hosted Pb-Zn deposits: insight from metal and halogen geochemistry of individual fluid inclusions. Geology 41, 679–682.
Goldfarb, R.J., Hofstra, A.H., Simmons, S.F., 2016. Critical elements in Carlin, epithermal, and orogenic gold deposits. In: Rare Earth and Critical Elements in Ore Deposits, 18, pp. 217–244.
Gray, C.M., 1984. An isotopic mixing model for the origin of granitic rocks in southeastern Australia. Earth Planet. Sci. Lett. 70, 47–60.
Groff, J.A., Heizler, M.T., McIntosh, W.C., Norman, D.I., 1997. 40Ar/39Ar dating and mineral paragenesis for Carlin-type gold deposits along the Getchell trend, Nevada, Evidence for Cretaceous and Tertiary gold mineralization. Econ. Geol. 92, 601–622.
Grunsky, E.C., Arne, D., 2020. Mineral-resource prediction using advanced data analyticls and machine learning of the QUEST-South stream-sediment geochemical data, southwestern British Colombia, Canada. Geochem.: Explor., Environ., Anal. 21, 054.
Hall, C.M., Simon, Grigore, Kesler, S.E., 1997. Age of mineralization at the Twin Creeks SHMG deposit, Nevada. In: Society of Economic Geologists Guidebook Series, 28, pp. 151–154.
Hawkes, H.E., 1976. The downstream dilution of stream sediment anomalies. J. Geochem. Explor. 6, 345–358.
Heinrich, C.A., 2005. The physical and chemical evolution of low-salinity magmatic fluids at the porphyry to epithermal transition: a thermodynamic study. Mineral. Deposita 39, 864–889.
Heitt, D.G., Dunbar, W.W., Thompson, T.B., Jackson, R.G., 2003. Geology and geochemistry of the Deep Star gold deposit, Carlin trend, Nevada. Econ. Geol. 98, 1107–1136.
Henkelman, C.A., 2004. Pyrite Geochemistry Across the Betze-Post Deposit, Northern Carlin Trend, Nevada [Ph.D. thesis]. University of Nevada, Las Vegas, 163 p.
Henry, C.D., Boden, D.R., 1998. Eocene magmatism: the heat source for Carlin-type gold deposits of northern Nevada. Geology 26, 1067–1070.
Hickey et al., n.d.Hickey, K.A., Barker, S.L.L., Dipple, G.M., Arehart, G.B., Donelick, R. (n.d.), The brevity of hydrothermal fluid flow revealed by thermal halos around giant gold deposits: Implications for Carlin-type gold systems: Economic Geology, v. 109, p. 461–1487.
Hofstra, A.H., 1994. Geology and Genesis of the Carlin-type Gold Deposits in the Jerritt Canyon District, Nevada. Unpublished Ph.D. thesis. University of Colorado, Boulder, 719 p.

Hofstra, A.H., 1995. Timing and duration of Carlin-type gold mineralization in Nevada and Utah—relation to back-arc extension and magmatism. Geol. Soc. Am. Abstr. Programs 27 (6), A329.
Hofstra, A.H., Cline, J.S., 2000. Characteristics and models for Carlin-type gold deposits. Rev. Econ. Geol. 13, 163–220.
Hofstra, A.H., Snee, L.W., Rye, R.O., Folger, H.W., Phinisey, J.D., Loranger, R.J., Dahl, A. R., Naeser, C.W., Stein, H.J., Lewchuk, M., 1999. Age constraints on Jerritt Canyon and other Carlin-type gold deposits in the western United States—relationship to Mid-Tertiary extension and magmatism. Econ. Geol. 94, 769–802.
Holley, E.A., Lowe, J.A., Johnson, C.A., Pribil, M.J., 2019. Magmatic-hydrothermal gold mineralization at the Lone Tree mine, Battle Mountain District, Nevada. Economic Geology 114 (5), 811–856.
Holley, E.A., Fulton, A., Jilly-Rehak, C., Johnson, C., Pribil, M., 2022. Nanoscale isotopic evidence resolves origins of giant Carlin-type ore deposits. Geology 50.
Huff, D., Holley, E., Guenthner, W., in review, The igneous history of the northern Battle Mountain District, Nevada and implications for the formation of sedimentary rock-hosted Au deposits. in review. Economic Geology.
Huff, D.E., Holley, E., Guenthner, W.R., Kaempfer, J.M., 2020. Fe-oxides in jasperoids from two gold districts in Nevada: characterization, geochemistry, and (U-Th)/He dating. Geochim. Cosmochim. Acta 286, 72–102.
Ilchik, R.P., Barton, M.D., 1997. An amagmatic origin of Carlin-type gold deposits. Econ. Geol. 92 (3), 269–288.
Johnson, C.A., Slack, J.F., Dumoulin, J.A., Kelley, K.D., Falck, H., 2018. Sulfur isotopes of host strata for Howards Pas (Yukon–Northwest Territories) Zn-Pb deposits implicate anaerobic oxidation of methane, not basin stagnation. Geology 46, 619–622.
Johnston, M.K., Ressel, M.W., 2004. Carlin-type and distal disseminated Au-Ag deposits: related distal expressions of eocene intrusive centers in north-central Nevada. In: Controversies on the Origin of World-class Gold Deposits, Part 1: Carlin-type Gold Deposits in Nevada, 59. Society of Economic Geologists Newsletter, pp. 12–14.
Kaplan, I.R., Rittenberg, S.C., 1964. Microbiological fractionation of sulphur isotopes. Microbiology 34, 195–212.
Keeler, D.A., 2010. Structural Reconstruction of the Copper Basin Area, Battle Mountain District, Nevada. Unpublished M.Sc. thesis. University of Arizona, 92 p.
Kesler, S.E., Ye, Z., Fortuna, J., Riciputi, L.C., 2003. In: Epithermal Carlin transition: Evidence for Magmatic Input to Carlin-type Deposits: Mineral Exploration and Sustainable Development, 1. Millpress, Rotterdam, pp. 493–494.
Kesler, S.E., Riciputi, L.C., Ye, Z., 2005. Evidence for a magmatic origin for Carlin-type gold deposits: isotopic composition of sulfur in the Betze-Post-Screamer Deposit, Nevada, USA. Mineral. Deposita 40 (2), 127–136.
King, C.A., 2011. Geology, Alteration, and Mineralization of the Elder Creek Porphyry System, Battle Mountain, Nevada. Unpublished M.Sc. thesis. The University of Arizona, Tucson, Arizona, 67 p.
King, C.A., 2017. Igneous Petrology, Geochronology, Alteration, and Mineralization Associated With Hydrothermal Systems in the Battle Mountain District, Nevada. University of Arizona. PhD thesis.
Kizis, J.A., Bruff, S.R., Crist, E.M., Mough, D.C., Vaughan, R.G., 1997. Empirical geologic modeling in intrusion-related gold exploration: an example from the Buffalo Valley area, northern Nevada. SEG Newsletter 30, 1, 6–13.
Krouse, H.R., Coplen, T.B., 1997. Reporting of relative sulfur isotope-ratio data (technical report). Pure Appl. Chem. 69 (2), 293–296.
Large, R.R., Bull, S.W., Maslennikov, V.V., 2011. A carbonaceous sedimentary source-rock model for Carlin-type and orogenic gold deposits. Econ. Geol. 106 (3), 331–358.
Lesher, C.M., Burnham, O.M., 2001. In: Multicomponent Elemental and Isotopic Mixing in Ni–Cu(– PGE) ores at Kambalda, Western Australia, Canadian Mineralogist, 39, pp. 421–446.
Li, Y., Liu, J., 2006. Calculation of sulfur isotope fractionation in sulfides. Geochim. Cosmochim. Acta 70 (7), 1789–1795.
Meinert, L.D., 2000. Gold in skarns related to epizonal intrusions. Rev. Econ. Geol. 13, 347–375.
Moore, J.W., Semmens, B.X., 2008. Incorporating uncertainty and prior information in stable isotope mixing models. Ecol. Lett. 11, 470–480.
Mortensen, J.K., Thompson, J.F.H., Tosdal, R.M., 2000. U-Pb age constraints on magmatism and mineralization in the northern Great Basin, Nevada. In: Geological Society of Nevada, Geology and Ore Deposits 2000: The Great Basin and Beyond Symposium, Reno/Sparks, Nevada, May 15-18, 2000, Proceedings, pp. 419–438.
Muntean, J.L., Cline, J.S., Simon, A.C., Longo, A.A., 2011. Magmatic-hydrothermal origin of Nevada's Carlin-type gold deposits. Nat. Geosci. 4, 122–127.
Neff, T.R., 1973. Emplacement of a dike swarm in the Buffalo Mountain pluton, Nevada. Geol. Soc. Am. Bull. 84, 3689–3696.
Ohmoto, H., Rye, R.O., 1979. Isotopes of sulfur and carbon. In: Barne, H.L. (Ed.), Geochemistry of Hydrothermal ore Deposits, pp. 509–567.
Parnell, A.C., Inger, R., Bearhop, S., Jackson, A.L., 2010. Source partitioning using stable isotopes: coping with too much variation. PLoS ONE 5 (3), e9672.
Parnell, A.C., Phillips, D.L., Bearhop, S., Semmens, B.X., Ward, E.J., Moore, J.W., Jackson, A.L., Grey, J., Kelly, D.J., Inger, R., 2013. Bayesian stable isotope mixing models. Environmetrics 24, 387–399.
Perry, R., Visher, M., 2016. Major Mines of Nevada 2015, Nevada Division of Minerals, Nevada Bureau of Mines and Geology.
Phillips, D.L., Gregg, J.W., 2001a. Uncertainty in source partitioning using stable isotopes. Oecologia 127, 171–179.
Phillips, D.L., Gregg, J.W., 2001b. Uncertainty in source partitioning using stable isotopes (erratum). Oecologia 128, 304.
Phillips, D.L., Gregg, J.W., 2003. Source partitioning using stable isotopes: coping with too many sources. Oecologia 136, 261–269.
Phillips, D.L., Newsome, S.D., Gregg, J.W., 2005. Combining sources in stable isotope mixing models: alternative methods. Oecologia 144, 520–527.
Phillips, D.L., Inger, R., Bearhop, S., Jackson, A.L., Moore, J.W., Parnell, A.C., Semmens, B.X., Ward, E.J., 2014. Best practices for use of stable isotope mixing models in food-web studies. Can. J. Zool. 92, 823–835.
Reid, R.F., Nicholes, J., Kofoed, R., McComb, M., Sechrist, K.J., 2010. In: Steinenger, Pennell (Eds.), Buffalo Valley Gold Mine: Porphyry Copper, Gold Skarn or Distal Disseminated Precious-metal Deposit, Great Basin Metallogeny, 1. Geological Society of Nevada.
Ressel, M.W., Henry, C.D., 2006. Igneous geology of the Carlin trend, Nevada: development of the Eocene plutonic complex and significance for Carlin-type gold deposits. Econ. Geol. 101 (2), 347–383.
Ressel, M.W., Noble, D.C., Henry, C.D., Trudel, W.S., 2000. Dike-hosted ores of the Beast deposit and the importance of Eocene magmatism in gold mineralization of the Carlin trend, Nevada. Econ. Geol. 95, 1417–1444.
Richards, J., 2011. In: Hidden Gold: Nature Geoscience, 4, pp. 73–74. Rottier, B., Kouzmanov, K., Casanova, V., Bouvier, A.S., Baumgartner, L.P., Wälle, M., Fontboté, L., Tracking fluid mixing in epithermal deposits - Insights from in-situ δ18O and trace element composition of hydrothermal quartz from the giant Cerro de Pasco polymetallic deposit, Peru, Chemical Geology, v. 576, 120277.
Rottier, B., Kouzmanov, K., Casanova, V., Bouvier, A.-S., Baumgartner, L.P., Walle, M., Fontbote, L., 2021. Tracking fluid mixing in epithermal deposits – Insights from in-situ δ18O and trace element composition of hydrothermal quartz from the giant Cerro de Pasco polymetallic deposit, Peru. Chem. Geol. 576, 120277.
Schwinn, G., Wagner, T., Baatartsogt, B., Markl, G., 2006. Quantification of mixing processes in ore-forming hydrothermal systems by combination of stable isotope and fluid inclusion analyses. Geochim. Cosmochim. Acta 70, 965–982.
Seedorff, E., Barton, M.D., 2004. Enigmatic origin of Carlin-type deposits: an amagmatic solution?. In: Society of Economic Geologists Newsletter, 59, pp. 14–18.
Semmens, B.X., Ward, E.J., Moore, J.W., Darimont, C.T., 2009. Quantifying inter- and intra-population niche variability using hierarchical Bayesian stable isotope mixing models. PLoS ONE 4, e6187.
Sillitoe, R.H., Bonham Jr., H.F., 1990. Sediment-hosted gold deposits: distal products of magmatic-hydrothermal systems. Geology 18 (2), 157–161.
Stewart, J.H., McKee, E.H., 1977. Geology and mineral deposits of Lander County, Nevada. In: Nevada Bureau of Mines and Geology Bulletin, 88, p. 106.
Stock, B., 2022. MixSIAR GitHub. https://github.com/brianstock/MixSIAR accessed February 24, 2022.
Stock, B.C., Jackson, A.L., Ward, E.J., Parnell, A.C., Phillips, D.L., Semmens, B.X., 2018. Analyzing mixing systems using a new generation of Bayesian tracer mixing models. PeerJ 6, e5096.
Theodore, T.G., 2000. Geology of pluton-related gold mineralization at Battle Mountain, Nevada. In: Monographs in Mineral Resource Science No. 2. Center for Mineral Resources, Tucson, The University of Arizona, p. 271.
Theodore, T.G., Silberman, M.L., Blake, D.W., 1973. Geochemistry and potassium-argon ages of plutonic rocks in the Battle Mountain mining district, Lander County, Nevada. In: United States Geological Survey Professional Paper 798-A, p. 24.
Theodore, T.G., Howe, S.S., Blake, D.W., Wotruba, P.R., 1986. Geochemical and fluid zonation in the skarn environment at the Tomboy—Minnie gold deposits, Lander County, Nevada. Journal of Geochemical Exploration 25 (1–2), 99–128.
Torres-Martínez, J.A., Mora, A., Knappett, P.S.K., Ornelas-Soto, N., Mahlknecht, J., 2020. Tracking nitrate and sulfate sources in groundwater of an urbanized valley using a multi-tracer approach combined with a Bayesian isotope mixing model. Water Res. 182, 115962.
Tretbar, D., Arehart, G.B., Christensen, J.N., 2000. Dating gold deposition in a Carlin-type gold deposit using Rb/Sr methods on the mineral galkhaite. Geology 28, 947–950.
U.S. Geological Survey. 2022 Final List of Critical Minerals. https://www.federalregister.gov/documents/2022/02/24/2022-04027/2022-final-list-of-critical-minerals.
Ward, E.J., Semmens, B.X., Schindler, D.E., 2010. Including source uncertainty and prior information in the analysis of stable isotope mixing models. Environ. Sci. Technol. 44, 4645–4650.
Zhang, J., Lin, Y., Yan, J., Li, J., Yang, W., 2017. Simultaneous determination of sulfur isotopes and trace elements in pyrite with a NanoSIMS 50L. Anal. Methods 9, 6653.